International Journal of Heat and Mass Transfer 209 (2023) 124124

Contents lists available at ScienceDirect

International Journal of Heat and Mass Transfer

journal homepage: www.elsevier.com/locate/hmt

Laser polarization associated periodic oscillation of thermal response in silicon nanotip

Xiaona Huang[1], Yibo Wang[1], Shugang Deng, Yanan Yue*

School of Power and Mechanical Engineering, Wuhan University, Wuhan, Hubei 430072, China

ARTICLE INFO

Article history:
Received 25 December 2022
Revised 1 March 2023
Accepted 20 March 2023

Keywords:
Thermal response
Raman thermometry technique
Silicon nanotip
Laser polarization

ABSTRACT

The nanotip's thermal response and its regulation are essential to tip-assisted nanoscale manufacturing. Laser polarization provides a promising solution for the dynamic tuning of laser energy absorption. However, the thermal response of nanotip under laser irradiation has yet to be fully understood. Here, the temperature and stress response of silicon nanotip under laser heating at different polarization angles is studied by Raman thermometry technique. The temperature oscillates between ~584 and ~742 K, with the polarization angle changing from 90 to 0°, showing sound dependence with laser polarization. Finite element simulations indicate that such oscillation effect of high temperatures is caused by the electric enhancement induced by the lightning rod effect and the low thermal conductivity of ~21 W/(m·K) due to the high temperature and the size effect of heat conduction. Meanwhile, polarization-dependent thermal stress occurs due to the large electric distribution gradient. The periodic oscillation of the temperature and stress with the polarization angle verifies the reversibility of the tuning process, which paves the way toward precise nano-manufacturing.

1. Introduction

Nanomanufacturing is pivotal in fabricating nanoelectronics with various functionalities [1,2]. A primary concern is assembling nanostructure units into nanodevices without changing their excellent physical properties. Nano-welding based on laser irradiated nanotip is an advanced manufacturing technique due to its advantages of controlled laser energy and efficient operation [3]. The hot tip is the important part whose temperature determines welding quality. For example, scanning probe microscopy (SPM)-based laser-irradiated probe has been demonstrated as an effective tool to fabricate nanoscale structures. The near-field enhancement around the tip provides a nanoscale hotspot [4]. Cui et al. induced near-field enhancement by irradiating atomic force microscopy (AFM) tip with a fiber optic probe, subsequently joining two carbon nanotubes with silver nanoparticles, resulting in a joint size of approximately 12 nm [5]. In these processes, the hot tip temperature is the most important parameter, while its accurate measurement and regulation are technically challenging due to the small scale of the nanotip and the resulting complicated thermal transport process. In addition, nanotip will expand even be damaged due to thermal stress caused by high-temperature gradient. Stress measurement and control is also essential for nanotip's normal performance.

There are relatively few techniques available for nanotip temperature measurement. Contact measurement is unrealistic due to nanotip's tiny scale. Noncontact methods, such as the infrared technique, are not feasible to probe temperatures on the nanoscale because of the diffraction nature of light [6,7]. Although previous works have demonstrated that embedded thermocouple was able to measure the temperature of the upper part of tip [8], the main challenge is the nanofabrication. Fluorescence signals excited from quantum dots whose size can be as small as sub-10 nm is another way to measure temperature at nanoscale [9]. However, in this scenario, quantum dots have a comparable size to the nanotip apex, which also prevents the measurement. Raman thermometry is a powerful technique to determine the sample temperature at nanoscale based on the excited Raman scattering signal from the laser irradiation area. Therefore, temperature measurement resolution can be readily determined by precisely controlling the laser shooting area. In this case, the tip apex temperature can be determined by adjusting the laser to irradiate the to-be-measured area, thus breaking the diffraction limit.

Indeed, Raman has been widely employed for determining the thermal properties of nanomaterials and nanostructures [10,11]. For instance, Yue et al. developed a steady-state electro-Raman thermal technique to characterize the thermal conductivity of multi-wall carbon nanotube bundles [12]. Raman can also be used

* Corresponding author.
E-mail address: yyue@whu.edu.cn (Y. Yue).
[1] X.H. and Y.W. contributed equally to this work.

https://doi.org/10.1016/j.ijheatmasstransfer.2023.124124
0017-9310/

to distinguish the temperature difference between graphene and substrate for analyzing interfacial thermal resistance [13]. Besides, transient Raman spectroscopy was also developed to determine the transient thermal property of nanomaterials [14–16]. Besides temperature, thermal stress can be simultaneously characterized by integrating the analysis of Raman peak shift and peak width [17]. Thermal stress measured by using Raman was also implemented for a few years. For instance, Gan et al. characterized the change in surface stress in microscale silicon samples in response to externally applied stress at different temperatures using micro-Raman spectroscopy [18].

As to tip-enhanced Raman thermometry, recent works on ballistic thermal transport study of semiconductors with hotspots at a sub-10 nm scale have been reported [19,20]. Raman can be used to probe the temperature of the nanotip accordingly. Chen et al. characterized the temperature of a silicon tip under lateral laser irradiation. They found that the laser spot location largely influences the tip temperature [21]. Simulation results show that laser polarization greatly impacts near-field enhancement around the nanotip [22]. It can be easily thought that nanotip temperature could be different if the polarization angle of incident laser is different. However, experimental validation has yet to be reported, and the thermal stress of nanotip under these irradiation conditions still needs to be uncovered.

In addition, changing the polarization angle of laser beam could be an effective way to modulate the tip temperature as long as we fully understand the thermal response of the laser heating process. In this work, we rotate the laser beam to construct different polarization irradiation scenarios of the nanotip. The thermal response of the nanotip, not just temperature but also thermal stress under laser heating, is measured by using Raman thermometry simultaneously. We find that the temperature oscillates with the polarization angle showing sound dependence with laser polarization. Such oscillation is caused by the lightning rod effect induced electric enhancement and low thermal conductivity due to the high temperature and size effect of heat conduction. Based on this, our work aims to achieve the periodic oscillation of thermal response in silicon nanotips.

2. Experimental setup and details

The experiment is conducted using an AFM silicon nanotip purchased from MikroMasch Company. As shown in Fig. 1, the tip has a very sharp pyramid structure with a tip apex size at the nanoscale. In the experimental setup, the tip is fixed on a precisely controlled 3D micro stage to ensure the laser spot only covers the top end of the tip. In order to minimize the laser spot size, a 50 × microscope objective lens is used to focus the continuous laser (wavelength: 532 nm) to the nanotip apex. This laser is employed not only for heating the tip but also to excite Raman signal simultaneously (Fig. 1). A confocal spectrometer collects the scattered Raman signal to translate the temperature of the tip. A typical Raman spectrum excited from the silicon tip is shown in Fig. 2a. It can be seen that the peak is centered at ~520 cm^{-1} at room temperature. In order to get the tip temperature, a calibration experiment is conducted in advance to obtain the correlation between the Raman signal and temperature. Different features of the Raman peak can be employed in the measurement to determine the thermal responses. The most important features are the Raman peak shift and full width at half maxima (FWHM) of the peak [17,23]. Therefore, the measurement accuracy is highly dependent on the precision of Raman peak fitting. In our work, the Voigt function is chosen to fit Raman peak for better accuracy. Each fitting spectrum is averaged from four times of Raman acquisition to minimize measurement uncertainty.

During the measurement, a nanotip is placed along the x-axis and heated by focused laser incidence along the z-axis (Fig. 2b). The SEM image shows that the tip has a height of 15 μm with a tip apex radius of 10 nm and a half-cone angle of 10° The radius of the focused laser spot is ~12.5 μm. The nanotip position is carefully adjusted to make the laser beam just focused on the tip apex. More specifically, the nanotip is first moved along the x- and y-axis to ensure the laser beam irradiates the tip apex. After Raman acquisition, the nanotip is moved along the z-axis until Raman intensity reaches its maximum. From the SEM image, we can also find that the flank of the nanotip is smooth (Fig. 2c). The polarizer is adjusted to rotate from 30° to 210° (the rotation angle is denoted as φ). Such a range of angles enables us to study the thermal response of the nanotip with a whole period of polarization angles.

3. Results and discussion

3.1. Polarization-dependent light field enhancement

Fig. 3 demonstrates a significant correlation between Raman signal intensity and polarization angle (Blue line). Raman intensity shows a decreasing trend with φ in 30–90° and 180–210° and an increasing trend with φ in 90°–180°. When the polarization direction is parallel and perpendicular to the tip axis (φ equal to 180 and 90°), the Raman signal intensity reaches its maximum and minimum, respectively. Thus, changing polarization angle can modulate Raman signal intensity in a wide range. The maximum Raman intensity is 1.7 times its minimum value. The Raman in-

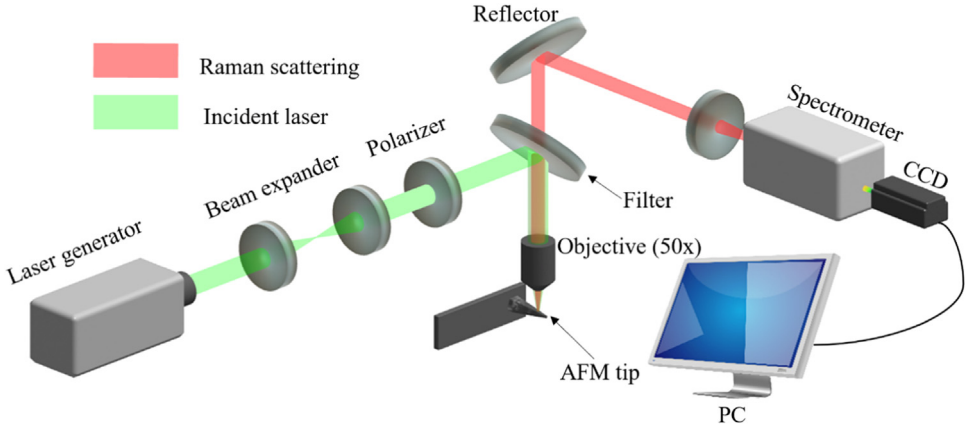

Fig. 1. Schematic of Raman-based experimental setup.

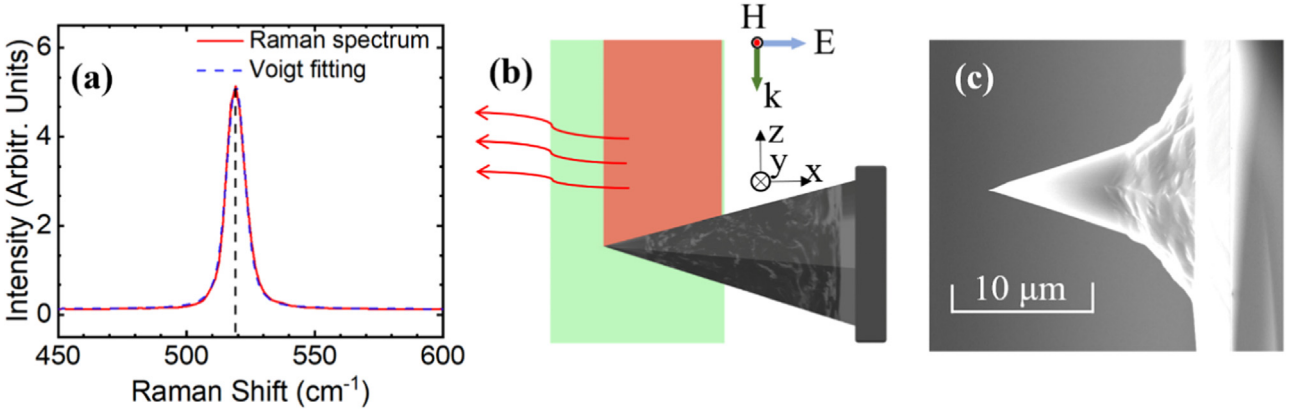

Fig. 2. (a) Characteristic peak in silicon Raman spectrum. (b) Simplified schematic of polarized laser incident direction and electric field direction. The green and red lights indicate incident laser and Raman scattering, respectively. (c) Side-view SEM image of the silicon nanotip.

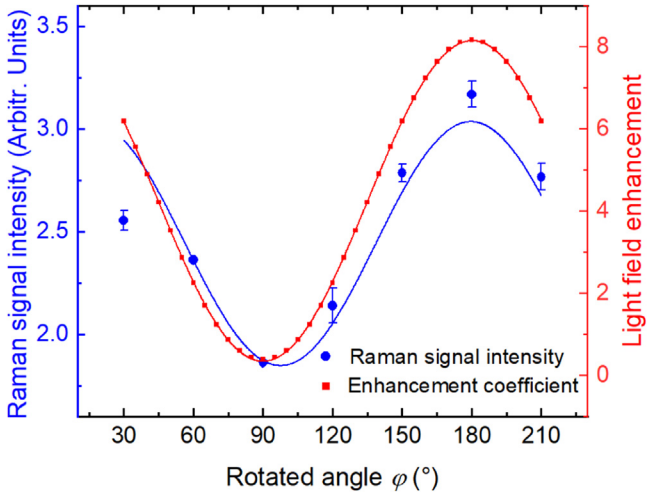

Fig. 3. Polarization angle related Raman signal intensity and light field enhancement of the silicon nanotip. The solid lines are fitted with a $\cos^2 \varphi$ curve.

tensities are close (2.55 and 2.77 Arbitr. Units) when φ is 30° and 210°, which shows the repeatability of the measurement because their polarization angles are the same. The Raman intensity as a function of polarization angle is well fitted by a $\cos^2 \varphi$ curve (Fig. 3). It is known that surface plasmon resonances can be efficiently excited by visible or near-infrared only for some noble metals, while the lightning-rod effect can occur in metallic and non-metallic probes. It indicates that the main reason for such Raman intensity variation of the nanotip is lightning rod effect. The Raman signal intensity enhancement may be explained by the fact that when the excitation field is perpendicular to the tip axis, the tip apex remains uncharged due to the opposite signs on either side. When the laser is aligned well with the tip axis, the tip apex shows the maximum surface charge density, resulting in an enhanced electric field [24].

Simulations based on the finite element method (FEM) and three-dimensional Maxwell governing equations are conducted to study the light field enhancement of the nanotip under polarized laser irradiation, and to further explore the mechanisms behind the effects of polarization angle on Raman signal intensity. The same three-dimensional nanotip model as that in experiments is built under Cartesian coordinate system, with an apex radius $r = 10$ nm, half cone angle $\theta = 10°$, and length $L = 500$ nm (Fig. 4). The perfect match layer (PML) boundary condition is applied to support the passage of electromagnetic waves in a reflection-free way. The initial temperature of the tip is settled as 292 K, and the wavelength of the electromagnetic wave is 532 nm. The dielectric constant at 532 nm of silicon nanotip is 17.237+0.43004i. The electric field amplitude is set at 1 V/m. Notably, incident light intensity depends on electric field intensity E as $I = 0.5c\epsilon_0 nE^2$, where c, ϵ_0, and n are light speed in a vacuum, vacuum permittivity, and refractive index, respectively. Thus, the square of electric field represents light field enhancement.

The light field enhancement shows a similar trend to Raman signal intensity and can fit well with a $\cos^2 \varphi$ curve (Fig. 3). Similar results have been reported that electric field enhancement depends on the incident electric field component along the tip axis while is independent of the perpendicular component [25]. As a consequence, the electric field enhancement depends on $\cos\varphi$. Meanwhile, incident light intensity is proportional to the square of electric field intensity E. Thus, the light field enhancement depends on $\cos^2 \varphi$, which has also been confirmed by our simulation results. The light field distribution of the nanotip (Fig. 4b) shows that there is little enhancement when the polarization angle is 90° ($\varphi = 90°$). The light enhancement gradually increases to 8.17 as the polarization angle decreases from 90 to 0° ($\varphi = 90° \sim 180°$). The light distribution is quite uniform without obvious enhancement at the polarization angle of 90° ($\varphi = 90°$). However, the nanotip exhibits significant local enhancement at the polarization angle of 45° and 0° ($\varphi = 135$ and 180°), with the highest value reaching 8 and 18, respectively. Our simulation shows little enhancement at the locations away from the tip apex, although covered by laser spot. This may be due to the fact that the lighting rod effect causes dipolar fields to concentrate near the sharp tip apex [26,27]. The $\cos^2 \varphi$ curve trend in the Raman signal intensity verifies the influence of polarization angle on light enhancement, which is well explained using our simulated results based on electromagnetic theory.

3.2. Temperature responses of silicon nanotip

FWHM broadens at a higher temperature due to a shorter phonon lifetime [10] and shows insensitivity to stress. Based on this, FWHM can be used to determine temperature. Although FWHM shows an almost linear relationship with temperature near room temperature, high-order anharmonicity cannot be ignored when temperature is high. FWHM involves terms proportional to the square of temperature in high-temperature limit [28,29]. Thus, FWHM versus temperature can be expressed using the quadratic function as:

$$\Gamma = \mathrm{B}(T_\Gamma - T_\mathrm{R})^2 + \mathrm{C}(T_\Gamma - T_\mathrm{R}) + \Gamma_\mathrm{R} \quad (1)$$

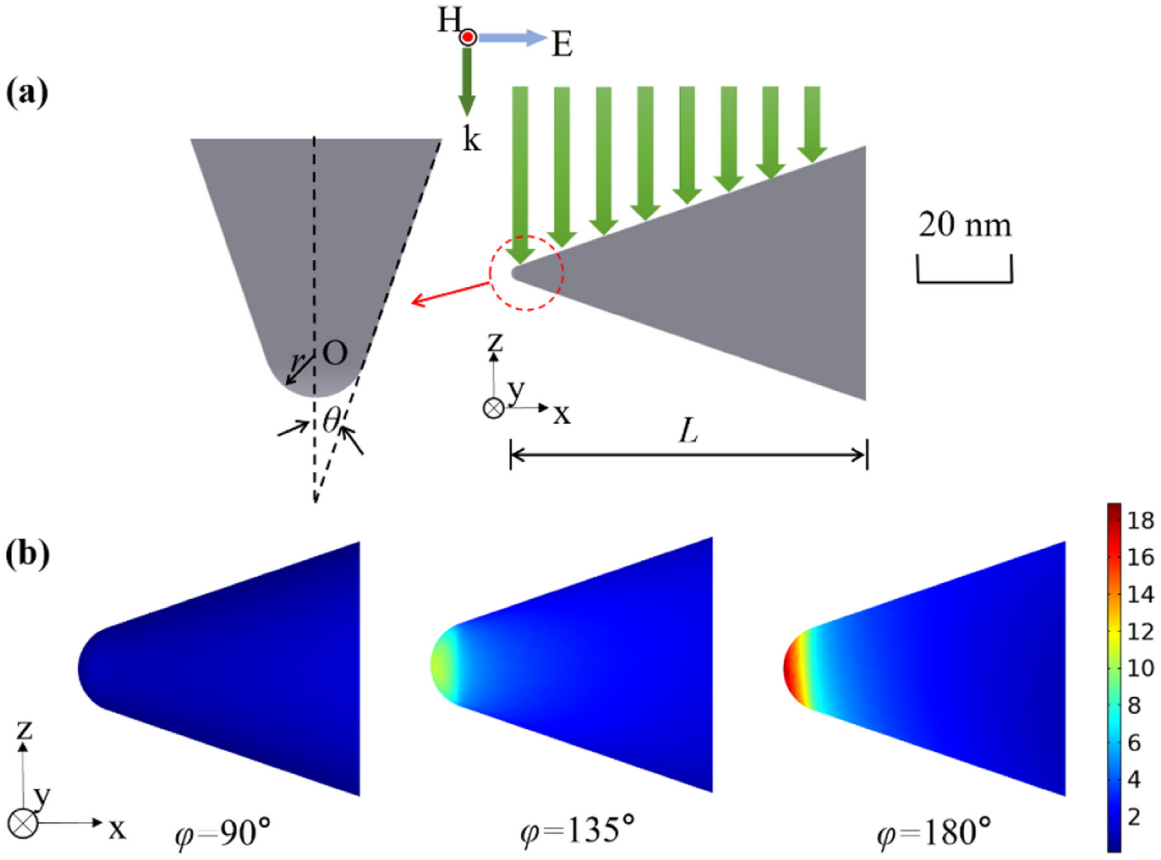

Fig. 4. (a) Geometric structure of the simulated nanotip. (b) Light field enhancement distribution projected to the x-z plane at different rotated angles inside the nanotip.

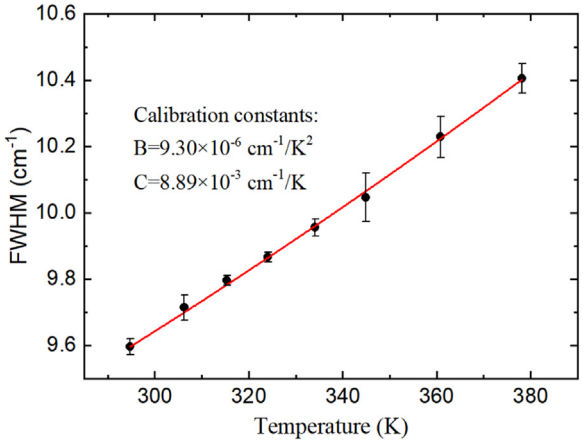

Fig. 5. FWHMs of silicon at different temperatures. The solid line is the fitted line using Eq. (1).

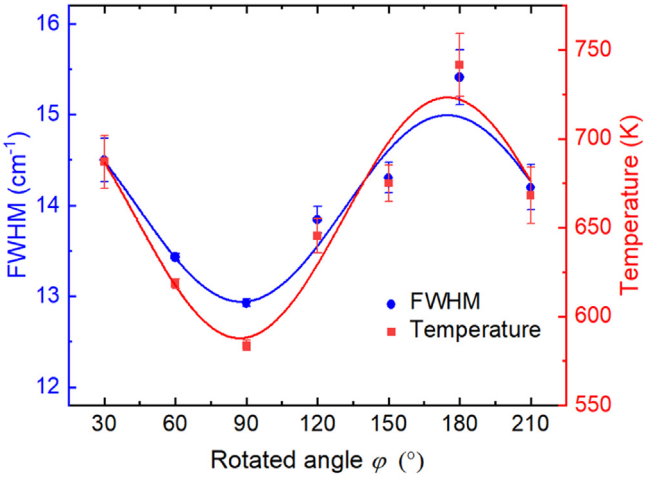

FIG. 6. Polarization angle dependent FWHM and temperature of the silicon nanotip. The solid lines are fitted with a $\cos^2 \varphi$ curve.

where B and C are calibrated parameters; T_R and T_Γ are ambient temperature and actual temperature obtained by FWHM fitting, respectively; Γ_R is FWHM at room temperature. Calibration is carried out in order to determine the calibration coefficients using an electrically heated silicon wafer since material size shows no effects on the temperature-dependent parameters. A small excitation laser power of 1 mW is set to prevent local heating. The calibrated parameters are obtained as $B = 9.30 \times 10^{-6}$ cm^{-1}/K^2 and C = 8.89 $\times 10^{-3}$ cm^{-1}/K by fitting FWHM using Eq. (1) (Fig. 5). The parameters extracted from our experiments are in the same order of magnitude as those from Beechem et al. [17] and Balkanski et al. [29], which shows the creditable of our results.

The FWHMs at different rotated angles and the accordingly nanotip temperatures based on the calibration curve are shown in Fig. 6. The trends of FWHM and temperature versus rotated angle are similar to that of light field intensity enhancement, because the heat generation rate in the nanotip is positively correlated with light field intensity as $\dot{q} = Ia$, where a is absorptivity. Similarly, thermal stress, depending on temperature gradient, is also polarization angle dependent, which will be discussed later. With the periodic change of the polarization angle, the nanotip temperature shows an obvious periodic oscillation. Laser power is 20 mW after passing through the polarizer. The nanotip temperature is around

584 and 742 K when the polarization direction is perpendicular ($\varphi = 90°$) and parallel ($\varphi = 180°$) to the tip axis, respectively. Our experimental results indicate that the maximum temperature difference caused by polarization direction change reaches ~158 K.

The temperature of a nanotip is determined by its heat generation rate and thermal properties. Incident laser acts on the nanotip in our experiments and serves as a heat source ($\dot{q}$). The heat generation rate positively correlates with the light field intensity, resulting in temperature oscillation as the polarization angle changes. In addition, equivalent thermal conductivity is estimated based on the FEM simulation of the nanotip and cantilever. The same laser power (20 mW) and action length (12.5 μm) as the experiments are set in our simulation. The equivalent absorptivity of the irradiated nanotip is calculated as 0.48 based on the Beer-Lambert law, $I(z) = I_0 \cdot e^{-\alpha z}$, where I_0 is laser intensity; z is penetration depth; α is absorption coefficient which is 12,233 cm^{-1} for silicon at 532 nm. The reflectivity is set as 0.37. Considering the effects of convection with the heat transfer coefficient of 10 W/(m^2·K) and irradiation, the equivalent thermal conductivity is ~21 W/(m·K), determined by making the nanotip temperature the same as that in experiments. The equivalent thermal conductivity of nanotip is much lower than the natural bulk value of 140 W/(m·K) [30]. The reason is attributed to two parts. One is high temperature since the thermal conductivity of natural bulk silicon significantly decreases at high temperatures due to the enhanced phonon scattering, which is ~50 W/(m·K) at 700 K [30]. The other is size effects which cannot be ignored in silicon microstructures. Regner et al. found that the mean free path in crystalline silicon spans 0.3–8.0 μm, and around 40% of its thermal conductivity comes from the phonons with a mean free path larger than 1 μm [31]. Even at 1000 K, computational results from Chen et al. [30] show that these phonons contribute about 25% to thermal conductivity. In our experiments, the largest section radius of the irradiated nanotip part is about 2.2 μm, and the tip apex radius is even down to 10 nm. The additional phonon boundary scattering of the nanotip limits the phonon mean free path and further reduces its equivalent thermal conductivity since phonon has such strong contributions with mean free paths larger than the nanotip's section radiuses. Thus, size effects exist in the nanotip heat transfer process even at a high temperature of ~700 K. We found that the low nanotip thermal conductivity causes significant temperature responses at different polarization angles and facilitates temperature regulation. Notably, our measured temperature is the average nanotip temperature covered by the laser beam. The local temperature can be much higher than the average one since simulations show that the maximum light field enhancement can reach approximately two times the average one at the rotated angle of 135 and 180° (Figs. 3 and 4).

3.3. Thermal stress of silicon nanotip

Unlike FWHM, Raman shift is affected by temperature and stress simultaneously. Raman shift can be expressed as:

$$\omega = \mathrm{W}(T_\Gamma - T_\mathrm{R}) + \mathrm{A}\sigma + \omega_\mathrm{R} \quad (2)$$

where ω_R is the peak position of Raman shift at room temperature; W and A are calibration constants of temperature and stress, respectively; σ is the averaged stress of the sample. The stress-related parameter A is given as -3.6 cm^{-1}/GPa from the previous study [32]. Similar to FWHM, calibration of Raman shifts at various temperatures is carried out using a silicon wafer to obtain the temperature-related parameter W, where the stress in the bulk silicon can be ignored. Fig. 7 shows that peak position linearly decreases with temperature, and W is estimated as -2.41×10^{-2} cm^{-1}/K. When the nanotip is heated with the laser beam, the free extension of the tip apex can generate significant stress.

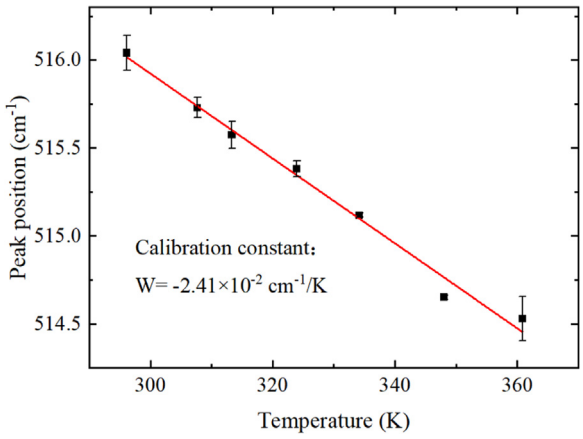

Fig. 7. Positions of Raman peak at different temperatures. The solid line is the fitted line using Eq. (2).

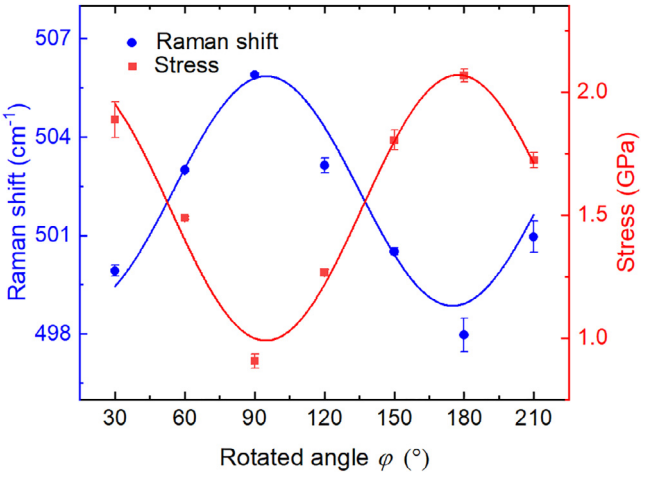

Fig. 8. Polarization angle dependent Raman shift and stress of the silicon nanotip. The solid lines are fitted with a $\cos^2 \varphi$ curve.

Thus, the Raman shift difference of nanotip can be expressed as $\Delta\omega = W(T_\Gamma - T_\mathrm{R}) + \mathrm{A}\sigma = W(T_\omega - T_\mathrm{R})$, where T_ω is obtained from Raman shift ignoring the stress. As a result, the average stress σ distributed on the tip can be expressed as $\sigma = W(T_\omega - T_\Gamma)/\mathrm{A}$.

Raman shift shows a redshift phenomenon with increasing temperature and stress. Therefore, for the irradiated nanotip, the trend of Raman shift with the rotated angle is opposite compared to Raman signal intensity, light field intensity, and temperature. Fig. 8 shows the measured Raman shift and calculated stress based on Eq. (2) and the calibration curve at different rotated angles. Raman shift shows the highest value when the polarization direction is perpendicular to the tip axis and the lowest value when parallel. The influence of stress on the Raman shift cannot be ignored when high stress exists in sample to ensure accurate measurement. Our results show that the contribution of stress and temperature to the Raman shift's change is comparable in nanotip. Non-negligible stress is caused by a great temperature gradient in nanotip. The thermal stress gradually increases as the polarization angle decreases from 90 to 0°. Its trend can be well fitted using a $\cos^2 \varphi$ curve similar to light field enhancement and temperature. The highest stress (~2.07 GPa) occurs at the maximum light field intensity and temperature, where the electric field gradient is greatest, while the lowest stress (~0.91 GPa) occurs at their lowest point.

For the heat transfer process of nanotip, on the one hand, a strong electric field gradient in nanotip with the maximum value

beneath the tip apex causes high heating energy density and high temperature at the tip apex. On the other hand, low thermal conductivity due to the size effect makes it difficult to conduct heat away from the tip apex, resulting in a high-temperature gradient and accordingly significant tensile thermal stress. Therefore, the high-temperature gradient is attributed to localized high light field intensity and low thermal diffusion capacity. In addition, the accuracy of our measurements is limited by Raman spectrometer resolution, which will bring errors in Raman peak position fitting. In our experiments, the main uncertainty of Raman measurement depends on the accuracy of the fitted characteristic peak wavenumber. Take the largest wavenumber uncertainty as an example. When the wavenumber error is 0.5 cm^{-1}, the maximum errors of temperature and stress are 17 K and 0.03 GPa, respectively. The errors could be reduced further by conducting more measurements, but the maximum temperature error only accounts for 2.3% of the temperature value.

3.4. Effects of thermal responses on nano-welding processes

As mentioned above, the nanotips' thermal responses are essential to consider during nano-welding processes. Our results show that we can regulate nanotip temperature by changing the polarization angle, which is more efficient than repeatedly adjusting laser power. In our experiments, nanotip temperature increases from ~584 to ~742 K when the polarization angle decreases from 90 to 0°, and the equivalent thermal conductivity of nanotip is ~21 W/(m·K) based on FEM simulations. However, thermal expansion caused by heat concentration in nano-joining process cannot be ignored. The linear expansion along tip axis can be estimated by $\Delta l/l = \alpha_T \Delta T$, where T is the absolute temperature and α_T is the thermal expansion coefficient of silicon, which is temperature dependent and can be expressed as [33]:

$$\alpha_T = \left(3.725\left(1-\exp\left(-5.88 \times 10^{-3}(T-124)\right)\right)+5.548 \times 10^{-4}T\right) \times 10^{-6} \quad (3)$$

We assume that the irradiated nanotip length is 12.5 μm in our experiments. The expansion length of the nanotip reaches ~16.2 and ~26.7 nm when the polarization angle is perpendicular and parallel to the tip axis, respectively. Similarly, previous study also shows that continuous laser leads to thermal expansion of probe nanotip along the tip axis, and even the cantilever parallel to the sample causes chaotic motion patterns [34]. Thus, thermal expansion should be considered to guarantee precise nanomanufacturing.

Materials fatigue when they reach their stress threshold, and high-stress conditions reduce their fatigue life [35]. As a brittle material, silicon has much lower tensile strength than its compressive and bending strengths. Experiments show that micro silicon has bending and tensile fatigue stresses of around 7.68 and 1.73 GPa at 295 K, respectively, and the specimen with a smaller size shows longer fatigue lives [36]. Besides, silicon is easier to fatigue at high temperatures caused of the decreased elastic constants. It can be thought that tensile stress determines the nanotip's failure, and tip temperature should be carefully controlled to prevent fatigue from high thermal stress and ensure service life. Our study shows that the thermal stress can be decreased from ~2.07 to ~0.91 GPa by only adjusting the polarization angle. In addition, nanotip geometry should be carefully designed to ensure accuracy in the nano-welding processes. Due to the size effect, the thermal conductivity of the nanotip decreases when its equivalent diameter decreases in nanoscale [37]. Accordingly, its temperature and thermal stress become higher with a smaller nanotip. Besides, Thomas et al. found that field enhancement of a tungsten tip is influenced by the tip's opening angle [38]. Therefore, an appropriate tip geometry should be used to obtain the desired temperature regulation effect.

4. Conclusions

To summarize, this work has demonstrated polarization angle-dependent thermal responses of silicon nanotip by Raman thermometry technique. Results show that Raman signal intensity and light field enhancement are consistent and polarization angle-dependent. Nanotip temperature is well regulated from around 584 to 742 K by decreasing the polarization angle from 90° to 0°. Combining experiments and FEM simulations, the equivalent thermal conductivity of the nanotip is estimated to be ~21 W/(m·K), indicating an obvious size effect, which contributes significantly to the high temperature and noticeable temperature difference of laser-heated nanotip. Meanwhile, a high electric field gradient in nanotip generates non-negligible thermal stress of ~2.07 and ~0.91 GPa at the polarization angle of 0 and 90°, respectively. Our results indicate that thermal response can be well regulated by changing laser polarization to avoid tip fatigue and ensure manufacturing precision during nano-welding processes.

Declaration of Competing Interest

The authors declare that they have no known competing financial interests or personal relationships that could have appeared to influence the work reported in this paper.

CRediT authorship contribution statement

Xiaona Huang: Methodology, Investigation, Formal analysis, Funding acquisition, Writing – original draft, Writing – review & editing. **Yibo Wang:** Data curation, Formal analysis, Writing – original draft, Writing – review & editing. **Shugang Deng:** Data curation, Formal analysis. **Yanan Yue:** Conceptualization, Funding acquisition, Supervision, Writing – review & editing.

Data availability

Data will be made available on request.

Acknowledgments

This study was supported by the financial support from the National Key Research and Development Program of China (No. 2019YFE0119900), the National Natural Science Foundation of China (No. 52076156), Natural Science Foundation of Hubei Province (No. 2021CFB120), and Fundamental Research Funds for the Central Universities (No. 2042022kf1020).

References

[1] H. Liu, T. Wang, Q. Jiang, R. Hogg, F. Tutu, F. Pozzi, A. Seeds, Long-wavelength InAs/GaAs quantum-dot laser diode monolithically grown on Ge substrate, Nat. Photonics 5 (7) (2011) 416–419.
[2] C. Wagner, N. Harned, Lithography gets extreme, Nat. Photonics 4 (1) (2010) 24–26.
[3] M. Xiao, S. Zheng, D. Shen, W.W. Duley, Y.N. Zhou, Laser-induced joining of nanoscale materials: processing, properties, and applications, Nano Today 35 (2020) 100959.
[4] M.L. Brongersma, N.J. Halas, P. Nordlander, Plasmon-induced hot carrier science and technology, Nat. Nanotechnol. 10 (1) (2015) 25–34.
[5] L. Yang, J. Cui, Y. Wang, C. Hou, H. Xie, X. Mei, W. Wang, K. Wang, Nanospot welding of carbon nanotubes using near-field enhancement effect of AFM probe irradiated by optical fiber probe laser, RSC Adv. 5 (70) (2015) 56677–56685.
[6] B. Nelson, W. King, Temperature calibration of heated silicon atomic force microscope cantilevers, Sens. Actuators A 140 (1) (2007) 51–59.
[7] Q. Sun, Z. Xue, Y. Chen, R. Xia, J. Wang, S. Xu, J. Zhang, Y. Yue, Modulation of the thermal transport of micro-structured materials from 3D printing, Int. J. Extreme Manuf. 4 (1) (2021) 015001.

[8] Y. Zhang, W. Zhu, F. Hui, M. Lanza, T. Borca-Tasciuc, M.Muñoz Rojo, A review on principles and applications of scanning thermal microscopy (SThM), Adv. Funct. Mater. 30 (18) (2020) 1900892.
[9] C. Li, Y. Yue, Fluorescence spectroscopy of graphene quantum dots: temperature effect at different excitation wavelengths, Nanotechnology 25 (43) (2014) 435703.
[10] R. Wang, S. Xu, Y. Yue, X. Wang, Thermal behavior of materials in laser-assisted extreme manufacturing: raman-based novel characterization, Int. J. Extreme Manuf. 2 (3) (2020) 032004.
[11] M. Bergler, K. Cvecek, F. Werr, M. Brehl, D. De Ligny, M. Schmidt, Cooling rate calibration and mapping of ultra-short pulsed laser modifications in fused silica by Raman and Brillouin spectroscopy, Int. J. Extreme Manuf. 2 (3) (2020) 035001.
[12] Y. Yue, G. Eres, X. Wang, L. Guo, Characterization of thermal transport in micro/nanoscale wires by steady-state electro-Raman-thermal technique, Appl. Phys. A 97 (1) (2009) 19–23.
[13] Y. Yue, J. Zhang, X. Wang, Micro/nanoscale spatial resolution temperature probing for the interfacial thermal characterization of epitaxial graphene on 4H-SiC, Small 7 (23) (2011) 3324–3333.
[14] Q.Y. Li, W.G. Ma, X. Zhang, Laser flash Raman spectroscopy method for characterizing thermal diffusivity of supported 2D nanomaterials, Int. J. Heat Mass Transf. 95 (2016) 956–963.
[15] Q.Y. Li, K. Xia, J. Zhang, Y. Zhang, Q. Li, K. Takahashi, X. Zhang, Measurement of specific heat and thermal conductivity of supported and suspended graphene by a comprehensive Raman optothermal method, Nanoscale 9 (30) (2017) 10784–10793.
[16] C. Li, S. Xu, Y. Yue, B. Yang, X. Wang, Thermal characterization of carbon nanotube fiber by time-domain differential Raman, Carbon N Y 103 (2016) 101–108.
[17] T. Beechem, S. Graham, S.P. Kearney, L.M. Phinney, J.R. Serrano, Invited Article: simultaneous mapping of temperature and stress in microdevices using micro-Raman spectroscopy, Rev. Sci. Instrum. 78 (6) (2007) 061301.
[18] M. Gan, V. Tomar, Surface stress variation as a function of applied compressive stress and temperature in microscale silicon, J. Appl. Phys. 116 (7) (2014) 073502.
[19] Y. Yue, X. Chen, X. Wang, Noncontact sub-10nm temperature measurement in near-field laser heating, ACS Nano 5 (6) (2011) 4466–4475.
[20] D. Huang, Q. Sun, Z. Liu, S. Xu, R. Yang, Y. Yue, Ballistic thermal transport at sub-10nm laser-induced hot spots in gan crystal, Adv. Sci. (2022) 2204777.
[21] X. Chen, X. Wang, Microscale spatially resolved thermal response of si nanotip to laser irradiation, J. Phys. Chem. C 115 (45) (2011) 22207–22216.
[22] H. Yin, J. Zhang, X. Wang, J. Cui, W. Wang, X. Mei, Recent progress in near-field tip enhancement: principles and applications, Phys. Status Solidi RRL 16 (4) (2022) 2100456.
[23] S. Deng, S. Xu, J. Gao, H. Wu, J. She, Y. Yue, Picosecond-resolved raman response of a si nanotip for probing temperature and thermal stress in the confined regime under laser heating, J. Phys. Chem. C 126 (4) (2022) 1922–1930.
[24] L. Novotny, R.X. Bian, X.S. Xie, Theory of nanometric optical tweezers, Phys. Rev. Lett. 79 (4) (1997) 645.
[25] X. Chen, X. Wang, Near-field thermal transport in a nanotip under laser irradiation, Nanotechnology 22 (7) (2011) 075204.
[26] P. Liao, A. Wokaun, Lightning rod effect in surface enhanced Raman scattering, J. Chem. Phys. 76 (1) (1982) 751–752.
[27] M. Asghari-Khiavi, B.R. Wood, P. Hojati-Talemi, A. Downes, D. McNaughton, A. Mechler, Exploring the origin of tip-enhanced Raman scattering; preparation of efficient TERS probes with high yield, J. Raman Spectrosc. 43 (2) (2012) 173–180.
[28] D. Jepsen, R. Wallis, Effect of quartic anharmonicity on the infrared absorption of alkali halide crystals, Phys. Rev. 125 (5) (1962) 1496.
[29] M. Balkanski, R.F. Wallis, E. Haro, Anharmonic effects in light scattering due to optical phonons in silicon, Phys. Rev. B 28 (4) (1983) 1928–1934.
[30] A.S. Henry, G. Chen, Spectral phonon transport properties of silicon based on molecular dynamics simulations and lattice dynamics, J. Comput. Theor. Nanosci. 5 (2) (2008) 141–152.
[31] K.T. Regner, D.P. Sellan, Z. Su, C.H. Amon, A.J. McGaughey, J.A. Malen, Broadband phonon mean free path contributions to thermal conductivity measured using frequency domain thermoreflectance, Nat. Commun. 4 (2013) 1640.
[32] I. De Wolf, Micro-Raman spectroscopy to study local mechanical stress in silicon integrated circuits, Semicond. Sci. Technol. 11 (2) (1996) 139.
[33] Y. Okada, Y. Tokumaru, Precise determination of lattice parameter and thermal expansion coefficient of silicon between 300 and 1500K, J. Appl. Phys. 56 (2) (1984) 314–320.
[34] J. Cui, J. Zhang, T. Barayavuga, X. Wang, X. He, L. Yang, H. Xie, X. Mei, W. Wang, Nanofabrication with the thermal AFM metallic tip irradiated by continuous laser, Integr. Ferroelectr. 179 (1) (2017) 140–147.
[35] J.F. Barbosa, J.A. Correia, R.F. Júnior, A.M. De Jesus, Fatigue life prediction of metallic materials considering mean stress effects by means of an artificial neural network, Int. J. Fatigue 135 (2020) 105527.
[36] T. Namazu, Y. Isono, Fatigue life prediction criterion for micro–nanoscale single-crystal silicon structures, J. Microelectromech. Syst. 18 (1) (2008) 129–137.
[37] L. Liang, B. Li, Size-dependent thermal conductivity of nanoscale semiconducting systems, Phys. Rev. B 73 (15) (2006) 153303.
[38] S. Thomas, G. Wachter, C. Lemell, J. Burgdörfer, P. Hommelhoff, Large optical field enhancement for nanotips with large opening angles, New J. Phys. 17 (6) (2015) 063010.